Metal Nanoparticle–Mesoporous Oxide Nanocomposite Thin Films

86

Paula C. Angelomé and M. Cecilia Fuertes

Contents

Abstract

Metal nanoparticles (NP) and mesoporous oxide thin films (MPF) can be combined to synthesize new nanocomposite materials (NP@MPF), with novel optical, catalytic, and sensing properties derived from the components combination and synergy. In this chapter, the usual synthesis methods together with the characterization techniques used to understand the composite structure will be described. The evolution of included NP and the nanocomposite stability during chemical, physical, or thermal treatments will be discussed. Finally, the most

P. C. Angelomé · M. C. Fuertes (✉)
Gerencia Química, Centro Atómico Constituyentes, Comisión Nacional de Energía Atómica, CONICET, San Martín, Buenos Aires, Argentina
e-mail: angelome@cnea.gov.ar; mfuertes@cnea.gov.ar

L. Klein et al. (eds.), *Handbook of Sol-Gel Science and Technology*,
https://doi.org/10.1007/978-3-319-32101-1_146

remarkable applications of these NP@MPF materials will be presented, including examples about their potential use in catalysis, photocatalysis, sensors (based on plasmonic and enhancement properties), and optical devices.

Introduction

The synthesis of ordered mesoporous oxides (MP) has experienced a great development during the last 20 years. These materials, whose pore diameters (from 2 to 50 nm) and array are carefully controlled, are prepared combining the self-assembly of amphiphilic molecules and sol-gel reactions. The supramolecular arrays formed by the amphiphilic molecules act as a template around which the oxide is formed, by the hydrolysis and condensation of an appropriate precursor. After thermal stabilization and template elimination, the final material presents high specific surface area and an ordered array of monodisperse pores. The field started its development with the MCM SiO_2 family in 1992 (Beck et al. 1992; Kresge et al. 1992), and since then, an enormous amount of MP materials with diverse chemical compositions has been developed (Kresge and Roth 2013; Lebeau et al. 2013; Gu and Schuth 2014; Li et al. 2014b). The materials can be obtained as powders, monoliths, membranes, fibers, and thin films, taking advantage of the versatility of the sol-gel route.

Mesoporous oxide thin films (MPF) are particularly interesting for many reasons, including high possibility of integration in current material processing technologies, flexibility of synthesis over very diverse substrates, and easy manipulation and extraction from a reaction medium (Innocenzi and Malfatti 2013). MPF are generally obtained by dip or spin coating techniques, using the evaporation-induced self-assembly methodology (Brinker et al. 1999). A wide variety of oxides have been synthetized to the date, including pure oxides (TiO_2, SiO_2, ZrO_2, Al_2O_3), mixed oxides (Ti–Si, Zr–Si, Zr–Ti, Zr–Ce), and hybrid oxides (Soler-Illia and Innocenzi 2006; Sánchez et al. 2008; Innocenzi and Malfatti 2013; Carretero-Genevrier et al. 2014). A wide variety of pore sizes and arrays can be easily obtained, particularly for SiO_2 and TiO_2 MPF, the most studied systems. These MPF are being tested for applications in fields as diverse as sensing, photocatalysis, solar cells, electronics, photonics, thermal insulating, photochromism, energy storage, and biological and medical applications (Innocenzi and Malfatti 2013).

A step forward is the combination of MPF with other nanomaterials, whose properties can complement or even improve the characteristics of the mesoporous oxide. Among all the possible composite materials that can be obtained, the combination of MPF with metal nanoparticles (NP) to form nanocomposites (that will be referred as NP@MPF) presents particular interest, due to the interesting properties of metallic NP.

The interest for metal NP increased during the past decade, motivated by their various special properties, which open potential applications in diverse fields (Xia et al. 2009). In particular, the catalytic and optical properties of NP have been

extensively studied. The use of NP in catalysis is related with their high specific surface area and their high surface reactivity, which drastically change when compared with bulk materials (Astruc et al. 2005; Schätz et al. 2010). On the other hand, NP optical properties are related to localized surface plasmon resonances (LSPR) (Bohren and Huffman 1983; Kreibig and Vollmer 1995), which give rise to intense extinction bands in the visible and NIR region in the case of Au, Ag, and Cu. Also related with LSPR, there is a high electric field enhancement at the NP surface (Moores and Goettmann 2006). The optical response of NP depends on their size, shape, and dielectric environment (refractive index of the medium, presence of neighboring NP, etc.) and, thus, can be tuned from synthesis (Liz-Marzan 2006). These interesting optical properties make the NP available for use in diverse fields such as sensing (Sepúlveda et al. 2009; Abalde-Cela et al. 2016), surface-enhanced Raman scattering (SERS) substrates (Álvarez-Puebla and Liz-Marzán 2010; Schlücker 2014), devices that require light confinement (Sperling et al. 2008; Atwater and Polman 2010), and medical applications (disease diagnosis and treatment, drug delivery devices, etc.) (Doane and Burda 2012; Howes et al. 2014; Jimenez de Aberasturi et al. 2015).

Due to the close relationship between synthesis, properties, and applications, the synthesis of NP by colloidal chemistry methods has been extensively developed (Xia et al. 2009). For the case of Au NP, spheres, nanorods, polyhedra, nanostars, and nanoplates are readily obtainable by controlling the reaction conditions (Grzelczak et al. 2008; Zhao et al. 2013; Li et al. 2014a; Carbó-Argibay and Rodríguez-González 2015). Also for Ag NP there are several examples of geometries available (Pastoriza-Santos and Liz-Marzan 2008; Xia et al. 2012). For the rest of the metals, the synthesis is more complex and less control over size and shape can be achieved (Xia et al. 2009).

Thus, metal NP and MPF can somehow complement each other, since the pores are complementary with the particles, both in size and potential applications. The obtained NP@MPF composites possess the intrinsic properties of each family, but also new features derived from the synergy between the components, mainly due to the huge interfacial contact between the metal and the oxide (Angelomé and Liz-Marzán 2014).

In this chapter, we will focus our attention towards NP@MPF nanocomposites. We will carefully describe the usual synthesis methods together with the characterization techniques used to understand the composite structure and properties. Finally, we will review some tested and potential applications reported for the synthesized materials.

Synthesis Methods

For the preparation of NP@MPF composites, three general approaches are used in most of the reported synthesis. These methods are schematically presented in Fig. 1 and will be described in the following subsections.

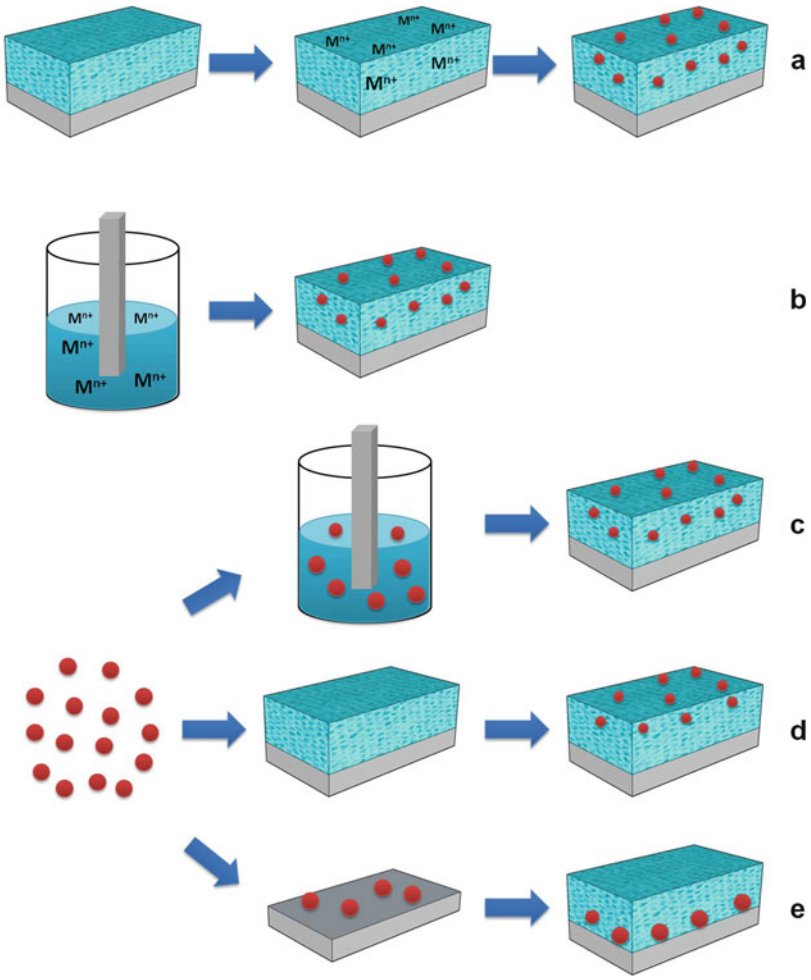

Fig. 1 Scheme of the different alternatives to prepare NP@MPF composites: (**a**) impregnation and reduction, (**b**) one-pot method, (**c**) pre-synthesized particles dispersed in the sol, (**d**) pre-synthesized particles incorporated in the films, and (**e**) thin film deposition on top of pre-synthesized particles

Impregnation and Reduction Approach

The impregnation and reduction approach is the most commonly used method to obtain NP@MPF composites. The general process is depicted in Fig. 1a: the particles are grown inside the porous structure once the pores are emptied. Thus, the NP are formed on the porous surface, partially or totally blocking the pores.

In this approach, the incorporation of the metallic salts and the subsequent reduction can be performed using a wide variety of techniques. For the adsorption of the metal salt, the tested techniques include: electrostatic interactions with the oxide (mainly for Ag(I) adsorption (Plyuto et al. 1999; Besson et al. 2003;

Andersson et al. 2005; Bannat et al. 2009; Horiuchi et al. 2009; Martínez et al. 2009; Nadar et al. 2011, 2013; Qi et al. 2011; Sayah et al. 2011; Destouches et al. 2014; Wolosiuk et al. 2014) but also performed for Au (Martínez et al. 2014; Violi et al. 2015)), specific interactions with amino groups modified oxides (for Au(III)) (Gu et al. 2005; Petkov et al. 2007; Cui et al. 2009a; Lu et al. 2011; Ding et al. 2014; Liu et al. 2015), and trapping within polyelectrolyte brushes (Calvo et al. 2010; Rafti et al. 2013). Although not all the published articles discuss about the subject, it is clear that for all these approaches the solution pH should be adequately adjusted to obtain the appropriate electrostatic attraction between the oxide walls and the metal salt. Thus, complexation of the cations is an alternative to ensure the proper interaction without compromising the stability of the ions.

The subsequent reduction can be performed by thermal treatment (Andersson et al. 2005; Sayah et al. 2011), UV irradiation (Fukuoka et al. 2002; Kumai et al. 2006; Martínez et al. 2009; Crespo-Monteiro et al. 2010; Nadar et al. 2013; Wolosiuk et al. 2014; Liu et al. 2015; Destouches et al. 2014), or by chemical reduction. The latter is the most usual path, and the most used reductants are formaldehyde (Bois et al. 2009; Fuertes et al. 2009; Wolosiuk et al. 2014), hydrogen gas (Plyuto et al. 1999; Fukuoka et al. 2002; Besson et al. 2003; Gu et al. 2005; Zhang et al. 2008; Cui et al. 2009a, b; Lu et al. 2011; Fang et al. 2012), and $NaBH_4$ (Bois et al. 2009; Calvo et al. 2010; Qi et al. 2011; Rafti et al. 2013; Ding et al. 2014; Martínez et al. 2014; Violi et al. 2015). A typical transmission electron microscopy (TEM) image of composites obtained by this methodology can be seen in Fig. 3c. It is important to note that, since the number of metal ions that can be adsorbed on the oxide's surface is limited, a single impregnation and reduction cycle is usually not enough to completely fill the pores. However, in most approaches it is possible to repeat the impregnation-reduction cycle several times, allowing a fine control over the amount of metal loaded (Martínez et al. 2014; Violi et al. 2015).

In this approach, the final particle size and shape depend on the pore size and connectivity. In most cases, spherical particles are obtained but also rod-shaped particles have been reported (see Fig. 3e, f) (Sayah et al. 2011). Moreover, the particle's shape can be modified by thermal treatment of the composite (Martínez et al. 2014).

An alternative of this method is the electrochemically induced impregnation and reduction (Pérez et al. 2004; Wu et al. 2006; Bannat et al. 2009; Kanno et al. 2012). For this purpose, the film needs to be deposited onto a conductive substrate such as ITO or Si, allowing its use as working electrode in an electrochemical cell. The metal loading is obtained by electrical potential application, while the electrode is immersed in the ion solution. This approach leads to a metal structure that fully replicates the pore array, which acts as a template (Wu et al. 2006; Kanno et al. 2012).

Another attractive possibility of this impregnation-reduction approach is the construction of metallic patterns onto the mesoporous structure. In this case, the reduction process should take place in a particular way that ensures the formation of metal NP only in specific regions of the MPF. For this purpose, Martínez et al. used a conventional lithography mask, to prepare Ag NP arrays inside TiO_2 MPF by UV exposure (Martínez et al. 2009). Ag is only formed where UV light reaches the surface, so patterns could be easily obtained in the submicron scale, as can be seen in

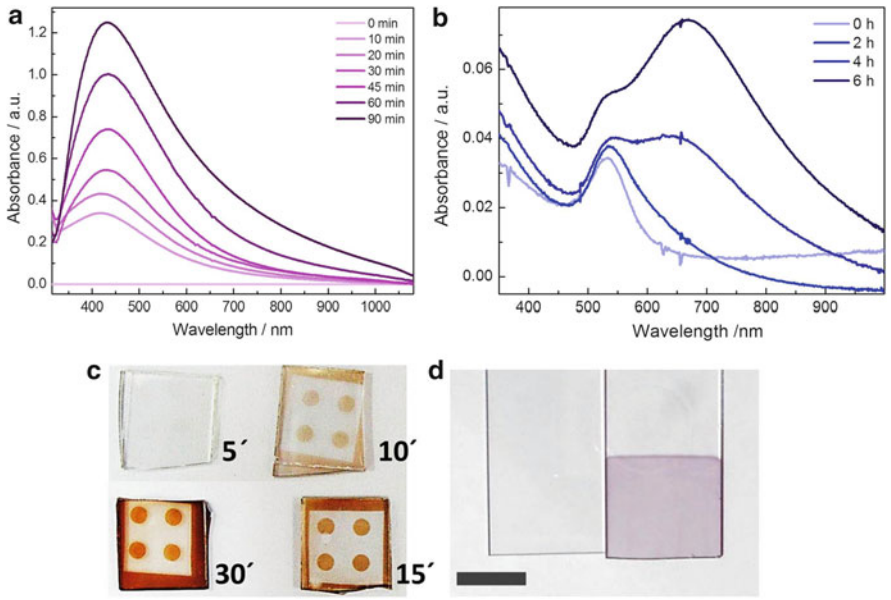

Fig. 2 (**a**) Ag NP plasmonic resonance for Ag@TiO_2 MPF. Ag NP were formed using chemical reduction of $AgNO_3$ solutions during different times. (**b**) UV–vis spectra of 15 nm Au NP@SiO_2 films before (0 h) and after (2, 4, 6 h) growth of Au tips through the pores. (**c**) Images of patterned Ag@TiO_2, showing the increase in the amount of Ag incorporated as a function of UV light irradiation time (Adapted from (Angelomé and Liz-Marzán 2014) with permission of Springer). (**d**) Images of TiO_2 MPF with (*right*) and without (*left*) Au NP included within the pores. The scale bar corresponds to 2 cm

Fig. 2c. This method is simple and low cost and, thus, very powerful. Interestingly, conductivity measurements performed in these nanocomposites indicate a three-dimensional connectivity between the embedded Ag NP (Martinez et al. 2010).

The use of continuous wave irradiation (Crespo-Monteiro et al. 2010; Destouches et al. 2014; Liu et al. 2015) or interferometric laser (Destouches et al. 2013) is an alternative approach to obtain patterned structures. In this case, the laser can be used to "write" the patterns directly onto the surface (Crespo-Monteiro et al. 2010; Destouches et al. 2013; Liu et al. 2015). Alternatively, by controlling the synthesis conditions, periodic arrays of Ag NP can be obtained initially. No masks are required, since the MPF acts as a waveguide to concentrate the light in particular positions where the reduction occurs (Destouches et al. 2014).

One-Pot Synthesis

In this approach, presented in Fig. 1b, a metal precursor is included in the sol mixture used to deposit the MPF. As the usual solution precursors are highly acidic, the metal salt is stable and the film preparation can be performed as usual. After deposition, the

porous structure and the particles are formed at the same time by using laser irradiation (Battie et al. 2010), X-ray irradiation (Malfatti et al. 2010, 2011), or conventional thermal treatments (Gu et al. 2004; Krylova et al. 2009; Battie et al. 2011; Chassagneux et al. 2011c).

The deep X-ray lithography method developed by Innocenzi's group is particularly interesting, since it allows obtaining patterned films. For this purpose, Au and Ag salts were added to Si sols, and freshly deposited films were treated with deep X-rays (in a synchrotron source) using appropriate masks (Malfatti et al. 2010, 2011). The irradiation leads to the formation of Au and Ag NP and also condenses the inorganic framework, thus allowing the obtention of patterned 3D mesoporous structures with NP inside them.

Using the one-pot approach, the obtained particles are generally small (due to the limited amount of metal salt that can be incorporated in the sol) and are distributed both inside the oxide walls and at the pores surface.

Use of Pre-synthesized Particles

This method presents several variations, but, in all of them, requires the preparation of metallic NP before their incorporation within the film. In general, NP are prepared by colloidal chemistry methods, starting from salt precursors, but other methodologies could be used. In this approach, both the size and the shape of the NP are defined prior to the composite preparation. This opens up the variability in the NP that can be included in the composites: nonspherical NP and diameters bigger than the pores are thus available. Nevertheless, due to the synthesis conditions, these methods usually do not allow high NP loadings.

Incorporation of Particles Within the Sol

In this methodology (schematized in Fig. 1c), metallic NP are incorporated in the sol before the thin film deposition. Thus, NP dispersion on the sol needs to be stable at least for the time required to prepare the MPF. Also, the NP size and shape and the amount that can be incorporated need to be controlled in order to allow the formation of smooth uniform films. These requirements make this method unusual, although some examples can be found in the literature (Kobayashi et al. 2001; Pérez-Juste et al. 2004; Goettmann et al. 2005; Cortial et al. 2006; Yang et al. 2008; Roldán et al. 2014, 2015). In the reported works, modification of the NP with organic ligands (Goettmann et al. 2005; Cortial et al. 2006), polymers (Roldán et al. 2015), or silica shells (Yang et al. 2008) has been tested to overcome the limitations of the method.

Related to this approach, Au clusters can be incorporated in the starting sols. The clusters are more easily stabilized than the NP, due to their size. After thermal treatment, Au NP are formed due to cluster collapse (Zhao et al. 2010).

Particle Diffusion Through the Film

This method, represented in Fig. 1d, is the most unusual since it requires the use of particles that are small enough to diffuse through the pores and necks of the MPF

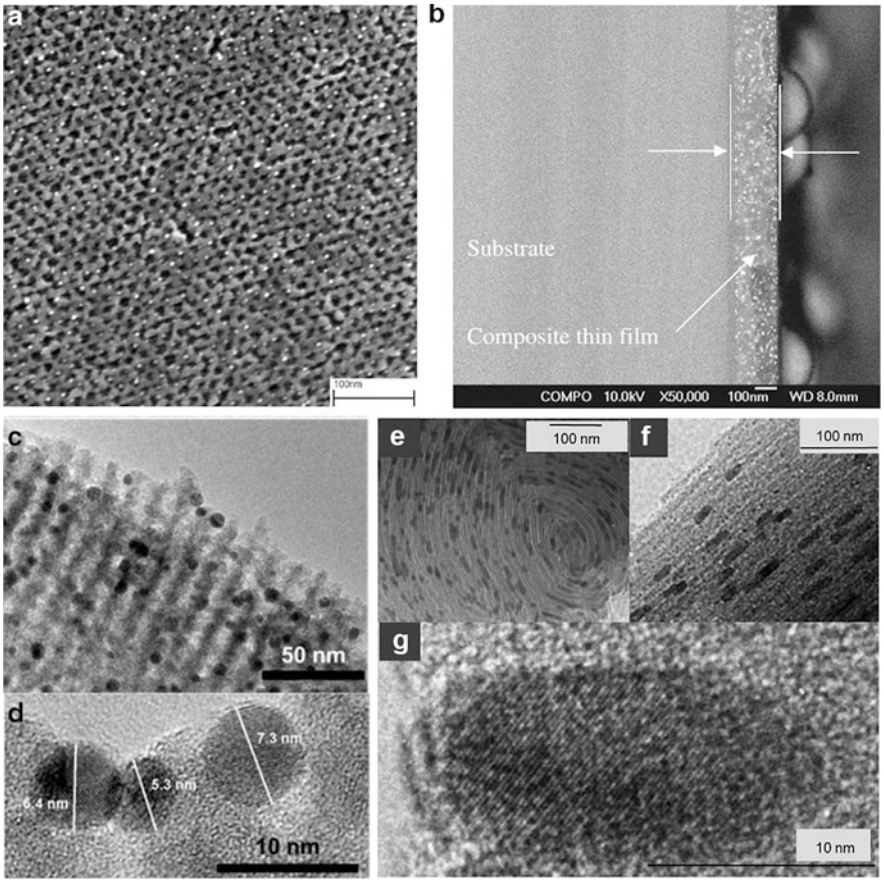

Fig. 3 (**a**) SEM top-down view of Au@TiO_2 (Reprinted with permission from (Patel et al. 2008). Copyright 2008 American Chemical Society). (**b**) Cross-sectional backscattered SEM image of Au@SiO_2 (Reprinted from (Lu et al. 2011) Copyright 2011, with permission from Elsevier). (**c**) TEM and (**d**) HRTEM images of Au@TiO_2 (Reprinted with permission from (Sánchez et al. 2013). Copyright 2013 American Chemical Society). TEM images of SiO_2 MPF with Ag nanorods: (**e, f**) top views and (**g**) high resolution (Reprinted from (Sayah et al. 2011) Copyright 2011, with permission from Elsevier)

(Patel et al. 2008; May et al. 2009; Mitra et al. 2012). An interesting approach to obtain such diffusion was presented by Patel et al. (2008): electrophoretic deposition was used to include 3.1 nm dodecanethiol stabilized Au NP into 10 nm perpendicular pores of a TiO_2 MPF (~150 nm thick) supported on conducting electrodes (see image of the composite in Fig. 3a). With this methodology, the Au NP loadings are high (21% wt), and the particles are present in the whole thin film thickness, as demonstrated by XPS. However, many of the Au nanocrystals reside near the top half of the film, and the NP concentration steadily decreased until reaching a very small concentration at the bottom of the film, in agreement with the expected

behavior. Also, the loading dependence on the NP diameter has been demonstrated (May et al. 2009).

Adhesion of Particles to a Substrate Followed by Film Deposition

This method has been recently reported (Angelomé and Liz-Marzán 2010; Angelomé et al. 2012; López-Puente et al. 2013, 2015) and represents a new approach, schematically shown in Fig. 1e. In the first step, metallic NP are prepared by usual colloidal methods. Afterwards, a sub-monolayer of the NP is chemically or electrostatically attached to a substrate and subsequently covered with the MPF. The method allows obtaining fully covered metallic NP (spheres, decahedra, rods, etc.) and well-ordered MPF oxides. The particles, whose shape and size can be finely tuned, remain accessible but also protected with the MPF, opening the way toward sensing applications (see below). Interestingly, the NP shape can be modified by using the NP as seeds and the films pores as templates. This method allows obtaining either larger NP or spiked NP, depending on the pore size of the MPF used (see the obtained spectra in Fig. 2b) (Angelomé et al. 2012; López-Puente et al. 2013).

Characterization

Characterization of metal NP@MPF generally includes both analysis of the MPF structure (porosity, pore size distribution, thickness, crystallinity) and the NP characteristics (particle size and shape, spatial distribution, crystallinity, pores' filling fraction). Besides, thermal, mechanical, and chemical stability studies that consider both the MPF and the NP are of great interest depending on the composite material application (Muraza et al. 2009; Rafti et al. 2013; Violi et al. 2015). This complex characterization is usually done by a combination of methods, including electronic microscopies, spectroscopies, and X-ray-based techniques. In this section we will described the most usual techniques used to characterize NP@MPF composites.

Optical Characterization

One of the most used techniques to study the formation and growth of metal NP with optical activity (Ag, Au, Cu) inside MPF is UV–visible spectroscopy. The experiment is very simple; in general, a transparent substrate is used and the NP@MPF is studied in transmission mode. The optical properties of NP are related to LSPR, which give rise to intense extinction bands in the visible and NIR (Kreibig and Vollmer 1995). There are numerous examples of UV–visible spectra in literature that show the formation and growth of Ag@SiO_2 (Plyuto et al. 1999; Besson et al. 2003; Dag et al. 2003; Bois et al. 2008, 2010; Hu et al. 2009; Battie et al. 2010; Qi et al. 2011; Sayah et al. 2011; Destouches et al. 2013), Ag@TiO_2 (Bois et al. 2009; Martínez et al. 2009; Crespo-Monteiro et al. 2010; Nadar et al. 2011, 2013;

Destouches et al. 2013), Au@SiO_2 (Goettmann et al. 2005; Gu et al. 2005; Calvo et al. 2010; Lu et al. 2011; Pedrueza et al. 2011; Angelomé et al. 2012), Au@TiO_2 (Zhang et al. 2008; Bannat et al. 2009; Cui et al. 2009a; Zhao et al. 2010; Pedrueza et al. 2011; Sánchez et al. 2013; Martínez et al. 2014), and other NP@MPF systems (Horiuchi et al. 2009; Krylova et al. 2009; Chassagneux et al. 2011a; Mitra et al. 2012; Leroy et al. 2013; Wolosiuk et al. 2014; Violi et al. 2015). Figure 2a shows the plasmon resonance absorption band for Ag NP inside TiO_2 MPF. In this case, Ag NP were formed using chemical reduction of $AgNO_3$ solutions in ethanol with formaldehyde during different times. The increment of the Ag plasmonic resonance intensity indicates the increase of the amount of NP inside the mesopores. For 1 h of reaction, the band widens as a result of NP–NP interaction.

UV–visible spectroscopy is also a powerful technique to detect changes in NP shape during the synthesis and post treatments (Angelomé et al. 2012; López-Puente et al. 2013). Figure 2b shows the UV–vis spectra of 15 nm Au spheres inside SiO_2 MPF. In this case, the composite film is immersed in a solution with Au^{+3}, ascorbic acid and CTAB, in order to obtain tips growing trough the pores. After 6 h of immersion in the growth solution, a second band is observed at longer wavelengths, revealing the presence of a second absorption mode, related to the branches (Angelomé et al. 2012; López-Puente et al. 2013). In this context, modeling the optical properties is a very useful tool to understand the changes in particles' size and shape. This methodology is commonly used to study NP in solution (Myroshnychenko et al. 2008), but there are just a few works that applied modeling as a tool to better understand the optical behavior of NP@MPF (Angelomé et al. 2012; Sánchez et al. 2013).

Colored films can be also observed by the naked eye or by using an optical microscope, in order to follow NP formation and composite evolution during synthesis (Bois et al. 2008, 2009, 2010; Bannat et al. 2009; Hu et al. 2009; Martínez et al. 2009; Malfatti et al. 2010; Nadar et al. 2011; Pedrueza et al. 2011; Sánchez et al. 2013). As an example, Fig. 2c shows optical images of patterned Ag@TiO_2 obtained by UV exposure of Ag^+ impregnated TiO_2 MPF using a lithography mask (Angelomé and Liz-Marzán 2014), and Fig. 2d presents optical images of Au NP@TiO_2 MPF composites.

Another optical technique for the characterization of NP@MPF composites is spectroscopic ellipsometry (SE) (Losurdo et al. 2009; Oates et al. 2011). This technique allows the determination of the thickness and optical constants, such as dielectric function and refractive index (Tompkins and McGahan 1999). For MPF containing metal NP, the model used to analyze SE measurements has to include the plasmonic properties of the nanocomposite. Patel et al. applied an anisotropic uniaxial model to analyze the SE results obtained for TiO_2 films following Au infusion (Patel et al. 2008). For this system, SE measurements of imaginary refractive index anisotropy indicate that Au nanocrystals are dispersed within the vertically aligned mesopores and distributed throughout the film. SE measurements were also performed on Ag@SiO_2 hybrid MPF; the authors found that composite's optical properties depend on host matrix optical properties and Ag concentration profile in the film (Battie et al. 2011).

In situ SE measurements of Au NP growing inside TiO_2 MPF were performed during thermal treatment. From these results, the kinetics of shape transformation of the included Au NP was studied, allowing the authors to develop a growth model (Sánchez et al. 2013). Finally, SE can be adapted to perform porosimetry (Baklanov et al. 2000; Boissiere et al. 2005): structural information of NP@MPF such as residual porosity and changes in mesopore sizes after NP inclusion can be obtained using this technique (Chassagneux et al. 2011b); this experimental setup also opens the possibility to study the plasmon response of the NP@MPF composite to changes in the environment (Sánchez et al. 2013).

For metal NP that does not present plasmonic resonance in the visible range of the spectra (Pd and Pt), it is necessary to use other techniques to study the inclusion of NP in the MPF, such as electron microscopies, X-ray diffraction (XRD), energy dispersive spectroscopy (EDS), or X-ray photoelectron spectroscopy (XPS) (Dag et al. 2003; Fukuoka et al. 2004; Gu et al. 2004; Cortial et al. 2006; Kumai et al. 2006; Wu et al. 2006; Petkov et al. 2007; Yacou et al. 2008; Muraza et al. 2009).

Structural Characterization

Structural characterization by scanning electron microscopy (SEM), TEM, atomic force microscopy (AFM), XRD, and small-angle X-ray scattering (SAXS) is used to determine important features for both MPF and NP. For MPF, these techniques allow the determination of mesopore order, pore sizes, and wall crystallinity; for NP, they permit the study of particle size and shape and the visualization of particles in the surface of MPF.

Depending on the NP synthesis method, nanocomposite films can have residual NP on its surface. In some cases, a careful cleaning is necessary to avoid undesired NP on surface after the synthesis (Wolosiuk et al. 2014). In other cases, post-treatment applied on the NP@MPF could generate NP on surface due to an expulsion of the metallic phase from the mesopores (Bois et al. 2009, 2010; Martínez et al. 2014). In this context, SEM, high-resolution SEM (HRSEM), and AFM studies of the nanocomposite films can give useful information related to NP on surface (Wu et al. 2006; Patel et al. 2008; Bois et al. 2009; Fuertes et al. 2009; May et al. 2009; Crespo-Monteiro et al. 2010, 2011; Cui et al. 2010; Martinez et al. 2010; Zhao et al. 2010; Nadar et al. 2011; Sayah et al. 2011; Destouches et al. 2014; Martínez et al. 2014; Wolosiuk et al. 2014). As an example, a top-down view SEM image of Au@TiO_2 is given in Fig. 3a. The Au nanocrystals (bright dots) are evenly dispersed across the TiO_2 MPF. Also, the mesopore sizes and pore order can be determined (pores are the darker region in the image). Besides, SEM and HRSEM studies of the nanocomposites in cross section can give useful information of NP sizes and spatial distribution along the film thickness (Cui et al. 2009a, b; Lu et al. 2011; Pedrueza et al. 2011; Destouches et al. 2014; Martínez et al. 2014) and MPF structural features (Wu et al. 2006; Kanno et al. 2012). Figure 3b shows a cross-sectional SEM image of Au NP@SiO_2 MPF, obtained from the reduction of $HAuCl_4$ in an amino silane-

modified MPF (Lu et al. 2011). Due to the much higher atomic number of Au than SiO_2, the white dots in the image represent the Au NP which were embedded and homogeneously dispersed in SiO_2 MPF, with a narrow size distribution. The average film thickness of the nanocomposite can also be measured from the cross-sectional SEM image.

Recent advances in electron microscopy techniques make possible the tridimensional observation of NP inside the matrix. Tomography measurements can be performed with a dual-beam focused ion beam/SEM system. The procedure involves the remotion of a thousand of successive slabs of matter with a Ga^+ ionic gun, and acquiring micrographs of the fresh cross sections sequentially revealed. Destouches et al. used this technique to study Ag NP inside TiO_2 MPF. The obtained 3D view of the nanocomposite shows that Ag NP form in a plane located near the film substrate interface and are rather spherical (Destouches et al. 2014).

TEM is the structural characterization technique most widely used to study mesoporous solids with or without metal NP (Bronstein 2003; Angelomé and Liz-Marzán 2014). This method enables the visualization of the mesoporous material structure (pore sizes and mesopore order), description of the spatial distribution of metal NP, and estimation of their size and shape (Andersson et al. 2005; Bois et al. 2010; Chassagneux et al. 2011a; Angelomé et al. 2012). As the electron contrast between MTF and metal NP is strong, information obtained from TEM images can be descriptive and even quantitative (Zhang et al. 2008; Horiuchi et al. 2009; Rafti et al. 2013; Sánchez et al. 2013; Liu et al. 2015). TEM images can be used to follow structural changes occurred in the MPF during the NP inclusion and to monitor changes in the amount, size, and shape of the NP during composite synthesis and posttreatment (Cui et al. 2009b, 2010; Battie et al. 2010; Angelomé et al. 2012; Destouches et al. 2013; López-Puente et al. 2013; Martínez et al. 2014). Cross-section TEM can provide information about NP location along MPF thickness (Besson et al. 2003; Petkov et al. 2007; Bannat et al. 2009; Battie et al. 2010; Bois et al. 2010; Destouches et al. 2013; Ding et al. 2014). Besides, TEM images of the NP@MPF composites give useful information about the structural integrity of both the NP and the MPF after the nanocomposite utilization for certain applications, as catalysis and sensors (Muraza et al. 2009; Rafti et al. 2013).

Some examples of TEM images of NP@MPF are shown in Fig. 3. Figure 3c presents an image of Au@TiO_2, synthesized by stepwise reduction of $AuCl_4^-$ with $NaBH_4$ inside the MPF (Sánchez et al. 2013; Martínez et al. 2014). Au NP (darker spots) present isotropic morphology and a diameter of around 5 nm. The meso-order can be also determined. Figures 3e and f show Ag nanorods inside SiO_2 MPF along the film thickness. These silver nanorods trapped in the film mesostructure have a width ranging from 7.8 and 8.9 nm and a length varying from 17 to 70 nm (Sayah et al. 2011).

High-resolution TEM (HRTEM) allows to obtain more detailed information on the guest NP, since the atomic structure of the metal can be elucidated. Some examples can be found in literature, for different metal NP (Fukuoka et al. 2002; Petkov et al. 2007; Cui et al. 2009b; Pedrueza et al. 2011; Mitra et al. 2012).

HRTEM picture of Fig. 3g displays (1 1 1) lattice fringes of *cubic face-centered* Ag and proves that the nanorods included in SiO_2 MPF are crystalline (Sayah et al. 2011). HRTEM gives also information on both particle size and particle location in the ordered mesoporous solids (Thomas et al. 2001; Bronstein 2003; Kumai et al. 2006; Bannat et al. 2009; Bois et al. 2010; Chassagneux et al. 2011a). Figure 3d shows an example of the TEM visualization of Au NP included in TiO_2 MPF. For this kind of nanocomposite, it was observed that the NP size is ultimately templated by the mesopore size and shape (Zhang et al. 2008; Sánchez et al. 2013).

Crystalline structures of metal NP and MPF walls can also be elucidated using diffraction techniques with electrons (selected area electron diffraction, SAED) and X-rays (XRD). SAED is a useful technique to study individual NP crystallinity, independently from the oxide matrix, as the NP can be previously found and observed using TEM. The obtained electron diffraction patterns from the NP or the MPF walls have to be indexed (Bois et al. 2008; Cui et al. 2009b; Krylova et al. 2009; Lu et al. 2011). XRD also allows the determination of crystalline structure for both NP and MPF (walls crystallinity) in one diffraction experiment (Andersson et al. 2005; Yacou et al. 2008; Krylova et al. 2009; Zhao et al. 2010; Roldán et al. 2014). In contrast to SAED that is a local technique, XRD results are representative of the whole sample since the data are collected on a large portion of the nanocomposite. When NP are crystalline, the corresponding Bragg diffraction peaks appearing in the diffractogram allow quantitative assessment of mean crystallite size that is similar to NP size if they are monocrystalline, as usually occurs; no information can be obtained on particle size distribution. If NP are amorphous or too small, they cannot be detected using this technique. Sometimes it is difficult to obtain a representative diffractogram in very thin films; in this case, low-angle X-ray incidence can be used in order to irradiate a bigger sample area.

In the case of MPF, X-ray diffractograms obtained at low diffraction angles (less than 5°2Θ) usually present intense Bragg peaks due to the pore periodicity in the direction normal to the surface of the substrate (Gibaud et al. 2006). The presence of metal NP within the mesoporous structure can sometimes be detected by a reduction of these Bragg reflection intensities. This intensity reduction is caused by the loss of pore arrangement order and the lowered reflection contrast between the framework and the pores, due to metal filling (Gu et al. 2005; Bois et al. 2008; Cui et al. 2009a; Lu et al. 2011). Using the same approach, SAXS with two-dimensional detection (2D-SAXS) can be used to characterize the mesoporous structure and to follow deviations of this structure when particles are formed within the MPF. 2D-SAXS method is the only straightforward and nonambiguous characterization technique to determine the mesoporous network structural periodic organization of MPF (Sánchez et al. 2008; Soler-Illia et al. 2012). After metal NP inclusion inside an ordered MPF, the SAXS signal can change or even disappear due to the random NP formation within the pores that disrupts the periodic electronic density which is the origin of the diffraction signal. In addition, the integrated intensity increases at low q values because of the low-angle X-ray scattering produced by metal NP (Fuertes et al. 2009; Wolosiuk et al. 2014).

Characterization of Metal Loading

A rigorous quantification of the metal loadings in mesostructured ordered thin films is not usually performed, but to know the amount of NP included is essential in some application as catalysis and optical devices. Analytical techniques such as EDS give an overall idea of composite film composition, while XPS, secondary ion mass spectroscopy (SIMS) (Zhang et al. 2008), and Rutherford backscattering (RBS) (Bois et al. 2009; Battie et al. 2011; Destouches et al. 2013) techniques can give details about NP location.

XPS is a suitable method to analyze the surface and in-depth atomic composition, the chemical state, and environment of the metallic and non reduced species (Ag^{+}, Au^{+3}, Au^{+1}, etc.) hosted in the MPF (Gu et al. 2004; Andersson et al. 2005). The distribution of NP through the complete MPF thickness can be elucidated using depth profile measurements (Patel et al. 2008; Horiuchi et al. 2009; May et al. 2009; Angelomé and Liz-Marzán 2010; Zhao et al. 2010). As ion sputtering can induce noticeable changes not only in the topography but also in the chemical composition of a multicomponent sample, special cares should be taken: bombarding the surface of the films with moderate energy, using the same conditions for all samples, and evaluating atomic ratio trends instead of absolute values.

The total metal NP content of composite thin film can be measured by EDS technique. The data obtained are qualitative; the metal content should be determined through averaging the collected data from different locations during SEM or TEM observations (Petkov et al. 2007; Martinez et al. 2010; Mitra et al. 2012). This technique can be used to evaluate changes in the metal NP loading after the application of thermal or chemical treatments to the nanocomposite material (Lu et al. 2011; Rafti et al. 2013). Figure 4a shows EDS spectra of TiO_2 MPF at different reaction times in a Ag^{+}/HCHO solution; the increase in the Ag signal indicates a larger amount of Ag NP included in the mesoporous matrix when reaction time is increased (Fuertes et al. 2009). Elemental maps of the sample surface can be performed to study patterned nanocomposites (Malfatti et al. 2010). Less common is to obtain an elemental map in a cross-sectioned sample, in order to evaluate NP location (Angelomé et al. 2012), or to elucidate local composition of different regions of nanocomposites (Destouches et al. 2013).

The amount of metal NP included inside the porous of MPF determined using EDS can be confirmed using X-ray reflectometry (XRR). XRR is a suitable method to determine NP inclusion in MPF, as it allows the simultaneous and direct determination of nanocomposite film density, thickness, and interfacial roughness from the reflectivity intensity variations with the X-ray incident angle (van der Lee 2000; Fuertes et al. 2009). XRR measurements are performed with the same experimental setup used to observe Bragg diffraction peaks related to mesopore order. Figure 4b shows the time evolution of XRR data obtained for a TiO_2 MPF treated in Ag^{+}/HCHO solution during different times. The patterns present a decay in the signal intensity at the total reflection critical angle, and a series of oscillations at higher angles, related to the film thickness (Kiessig fringes), can be observed for untreated MPF. The critical angle change with reaction time reflects the increment in film effective density due to the formation of metal NP inside MPF; the amount of metal

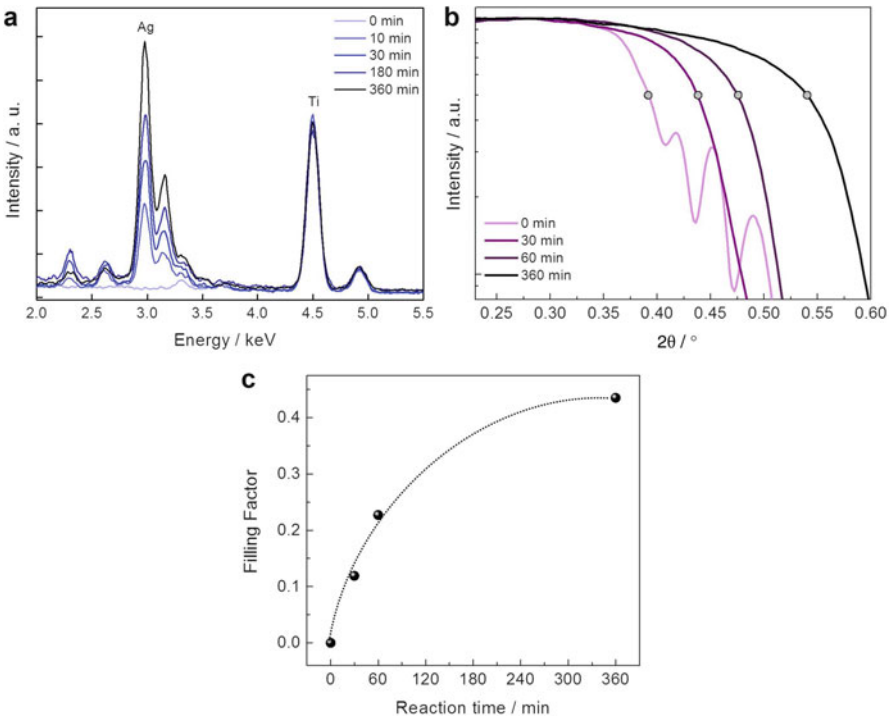

Fig. 4 (**a**) EDS spectra of TiO_2 MPF at different reaction times in Ag^+/HCHO solution. Ag and Ti signals are indicated. (**b**) Reflectivity data of TiO_2 (0 min) and Ag@TiO_2 MPF at different reaction times in Ag^+/HCHO solution. The critical angle is marked with a *circle* in each curve. (**c**) Pore filling factor of TiO_2 MPF with Ag NP at different reaction times, calculated from reflectivity data presented in (**b**). The *dotted line* was added for eye guiding

formed can be quantified from the calculated density values (Fuertes et al. 2009; Angelomé et al. 2010; Calvo et al. 2010; Wolosiuk et al. 2014; Violi et al. 2015). Figure 4c shows the evolution of the mesopore filling fraction with Ag NP for different reduction times, calculated considering the change in electronic density and the empty film porosity. Finally, the accessibility of the nanocomposite film to water can be also determined using this technique, by measuring changes in the nanocomposite's critical angle at low and high humidity (Fuertes et al. 2009). These kinds of studies are fundamental to understand the capacity of NP@MPF systems to detect analytes that reach NP inside the MPF matrix.

Applications

Although most of the works done so far has been focused on the synthesis and characterization of the NP@MPF composites, several examples of applications for such composites have been presented. In what follows, we will show some selected

examples of the most commonly presented applications, highlighting the advantages of using the composites.

Catalysis

Metal NP (particularly Pt and Pd, but also Au, Ag, and other transition metals) are widely used as catalysts in a large amount of organic reactions, and many examples have been reported about their use when supported onto mesoporous oxide powders (Sun and Bao 2008; White et al. 2009). The encapsulation of NP within MPF is a further step toward improving the composite features, in particular for a more efficient recovery and reuse than in the case of powders (Mitra et al. 2012; Violi et al. 2015). An example of such improvement is presented in Fig. 5, for the catalysis of the 4-nitrophenol reduction using Au NP@$Zr_{0.5}Ce_{0.5}O_2$ MPF, followed by UV–visible spectrometry. It can be clearly observed that the reaction proceeds only when the composite is introduced in the solution (Fig. 5c), demonstrating both the control over the reaction and the easy recovery of the catalyst. The reusability of the composite is also demonstrated (Fig. 5d) (Violi et al. 2015).

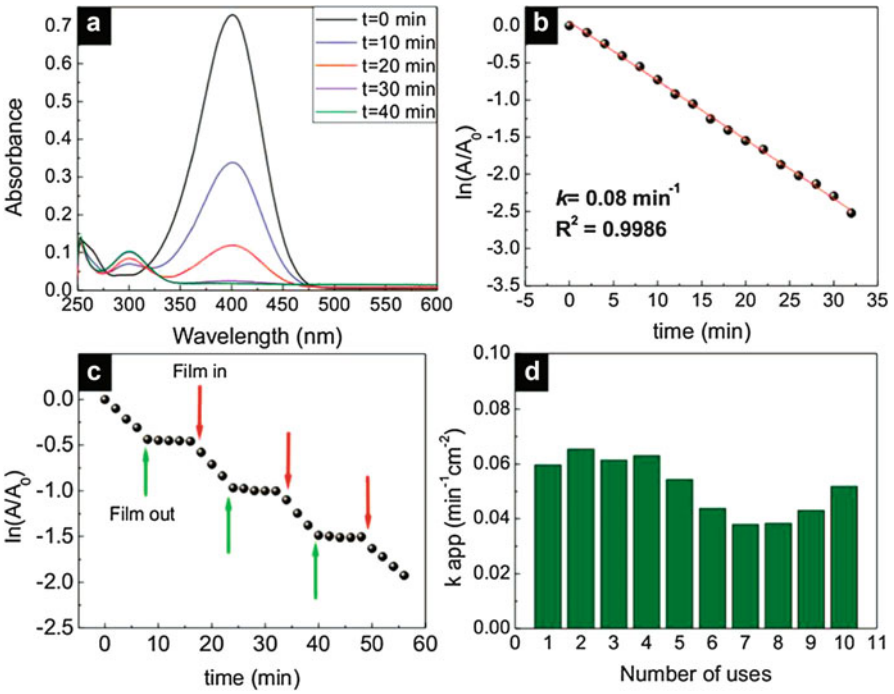

Fig. 5 4-Nitrophenol reduction catalysis by Au NP@$Zr_{0.5}Ce_{0.5}O_2$. (**a**) Spectra as a function of time. (**b**) Fit to first-order kinetics. (**c**) Leaching test: *green arrows* indicate film withdrawal, and *red arrows* indicate film reintroduction. (**d**) Catalyst reutilization (Reprinted with permission from (Violi et al. 2015). Copyright 2015 American Chemical Society)

Moreover, MPF can also influence the effectiveness of the NP, by adding extra selectivity or by confinement effects (Cortial et al. 2006; Muraza et al. 2009; Rafti et al. 2013). For example, Cortial et al. (Cortial et al. 2006) tested Pd NP@SiO_2 to catalyze the allylic amination of cinnamyl acetate by benzylamine and found that immobilized NP were three orders of magnitude more active than their homogeneous counterparts. Moreover, the regioselectivity was totally in favor of one of the possible products.

On the other hand, NP can improve the catalytic ability of MPF, as in the case of TiO_2 used as photocatalysts. In this system, when the oxide is modified with NP, a synergic effect takes place: the metal NP improves the electron flow from the TiO_2 surface to the metal, thereby suppressing electron–hole recombination, one of the main causes of activity loss. Thus, there are several examples in the literature in which Au or Ag NP were included within TiO_2 MPF in order to improve its photocatalytic performance (Andersson et al. 2005; Bannat et al. 2009; Zhao et al. 2010; Roldán et al. 2014, 2015). For example, Andersson et al. observed an apparent difference in reaction mechanism and initial activity for stearic acid photodegradation, when Ag NP are incorporated within TiO_2 MPF (Andersson et al. 2005). Au has also an improvement effect over the TiO_2 efficiency, as demonstrated by Bannat and et al. for the oxidation of NO (Bannat et al. 2009) and Zhao et al. for the degradation of organic dyes (Zhao et al. 2010).

Finally, another interesting example was recently reported by Roldán et al. (2014), who demonstrated the possibility of both improving the TiO_2 catalytic activity and adding a biocidal effect by Ag NP incorporation, resulting in a multifunctional composite.

Sensors

Metallic NP has been extensively studied for their use in sensors, mainly because of their attractive optical properties, particularly LSPR (Sepúlveda et al. 2009), and enhancement of Raman signals for SERS (Álvarez-Puebla and Liz-Marzán 2010; Schlücker 2014). Consequently, composites containing metallic NP and MPF have also been tested as sensors.

In the case of sensors based on LSPR, MPF can act as a support, as demonstrated by Goettmann et al. (2005) and Hu et al. (2009). The latter example is particularly interesting since the authors showed that it was possible to visually follow the oxidation and reduction of Ag NP incorporated within SiO_2 MPF, taking advantage of reversible appearance and disappearance of the characteristic brown color of Ag particles when exposed to reductive (H_2) and oxidative (air) gases.

Additionally, the LSPR band of Au decahedra was used to report the behavior of a solvent incorporated within the pores of the MPF that covered them, making possible to study solvent-oxide interactions. In this case the MPF is not a support, but the studied layer (Angelomé and Liz-Marzán 2010).

In the case of SERS sensors, again, the MPF can act as a support for Ag particles (Malfatti et al. 2011; Wolosiuk et al. 2014). Interestingly, when particles are obtained by impregnation and reduction approach, their distribution within the oxide is highly

uniform, and thus, the SERS signal is very reproducible along the sample (Fig. 6a). Besides that, several oxides with different chemical properties can be used as support (SiO_2, TiO_2, ZrO_2), paving the way toward SERS substrates with tailored properties (Wolosiuk et al. 2014).

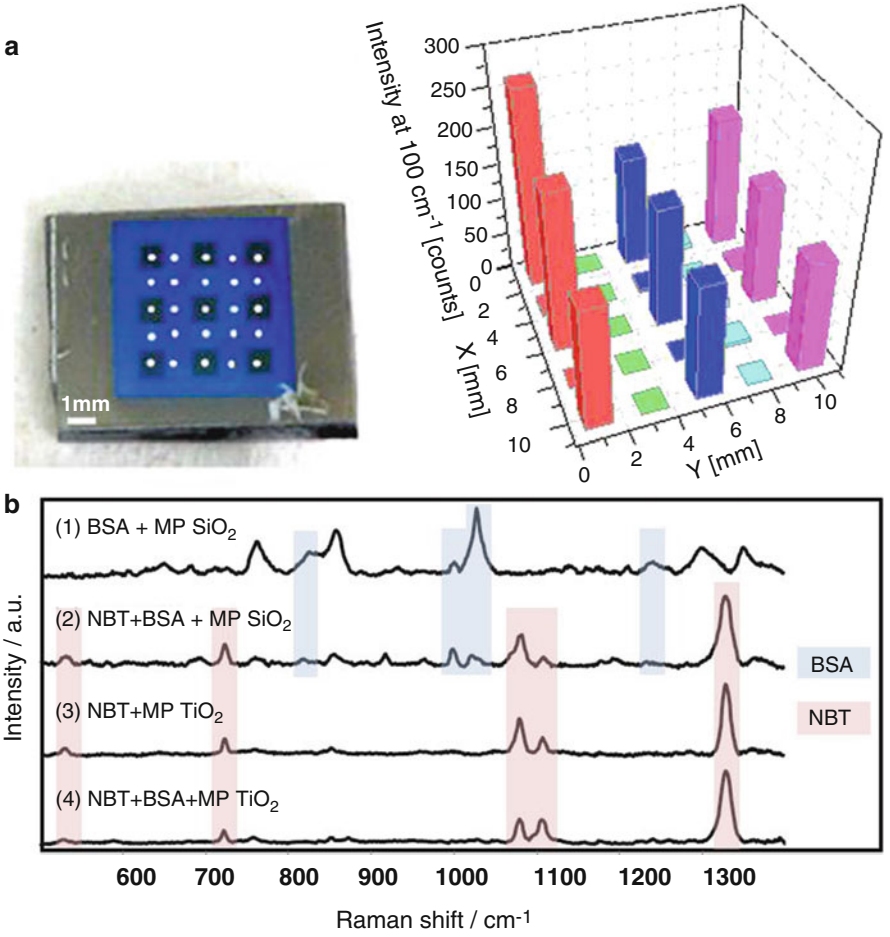

Fig. 6 (**a**) *Right side*: SERS intensity profile measured from the 4-mercaptopyridine peak at 1100 cm^{-1}, in Ag @TiO_2 composites prepared by UV exposure using a lithographic mask. *Left side*: optical image of the patterned sample showing in *gray*/*blue* the areas loaded/unloaded with Ag NP and in *white* the spots where the SERS spectra were measured (Adapted with permission from (Wolosiuk et al. 2014). Copyright 2014 American Chemical Society). (**b**) SERS spectra from 80 nm spiked Au NP covered with different films showing a size exclusion *proof of concept*. (*1*) Spectrum of BSA on SiO_2 MPF, (*2*) spectrum of NBT on SiO_2 MPF in the presence of BSA, (*3*) spectrum of NBT on TiO_2 MPF, and (*4*) spectrum of NBT on TiO_2 MPF in the presence of BSA. All solutions were prepared in PBS buffer (Adapted with permission from (López-Puente et al. 2013). Copyright 2013 American Chemical Society)

However, the porous structure of MPF also offers the possibility of filtering certain molecules by size or chemical interactions. In this sense, López-Puente et al. (2013) have reported the use of spiked Au spheres covered with TiO_2 MPF to detect a small molecule (4-nitrobenzenethiol, NBT) in the presence of a bigger molecule (bovine serum albumin (BSA) protein), which is also a typical molecule of biological media. As can be seen in Fig. 6b, for the TiO_2 MPF, a clean SERS signal of NBT is observed, even when BSA is present. However, when SiO_2 MPF are used, dissolution of the thin film occurs and both BSA and NBT are detected. In this approach, the NP provides the sensing capability while the MPF confers selectivity to the sensor. In a similar direction, the same authors (López-Puente et al. 2015) have demonstrated that the presence of specific functional groups in the pore network of the MPF allows control over the surface chemistry of the pores, tuning the sensor's selectivity. Amino-functionalized MPF were used to discern the presence of methylene blue (MB) in mixtures with acid blue (AB), with no need for sample pretreatment. Selective detection of MB was possible through entrapment of AB in the mesoporous matrix, based on its high affinity for amino groups. Moreover, the sensor selectivity was tuned by varying the solution pH.

As can be seen, although the examples presented so far are mainly *proof of concept*, the potential of nanocomposite films as sensors has been clearly demonstrated. More efforts are needed from now on to obtain prototypes for real applications.

Optical Devices

NP@MPF composites have novel optical properties due to the synergy between the metal NP and the porous oxide matrix. The design and study of these properties are of high interest regarding the advanced applications involved, including communication and information technology devices. Next, some selected examples of nanocomposites' optical properties are described.

Nonlinear Optics

Noble metal NP contained in dielectric matrix thin films have been investigated widely for their nonlinear optical properties, due to the enhancement of the local electric field at the region of the LSPR of the metal NP (Hamanaka et al. 2004). Materials with third-order optical nonlinearity are essential for light-controlled phase and refractive index modulation for applications in optical signal processing and nonlinear optical devices (Fang et al. 2012).

Initially, the composites designed for nonlinear optics were prepared by co-sputtering (Liao et al. 1997) or using the sol-gel method (Selvan et al. 2002), but the nanocomposites suffered from drawbacks due to uncontrollable NP size and spatial distribution (Cui et al. 2009a). Recently, several groups started to develop NP@MPF composites: the ordered mesoporous matrix ensures a high dispersion and a uniform distribution of the NP inside the films, and thus, the nonlinear optical properties can be carefully controlled. Using this approach, relatively high third-

order nonlinear optical susceptibilities ($\chi^{(3)}$) were obtained, for Au@TiO_2 (Cui et al. 2009b, 2010) and Au@SiO_2 MPF composites (Gu et al. 2005; Cui et al. 2009a; Lu et al. 2011; Fang et al. 2012). It was even possible to tune the $\chi^{(3)}$ value by controlling the amount of metal NP incorporated in the matrix (Lu et al. 2011); in this case, the high $\chi^{(3)}$ value is attributed to the very high metal content and homogeneous dispersion of NP with narrow size distribution (Cui et al. 2009a). In all cases, nonlinear optical properties of the nanocomposites were studied by the Z-scan technique.

Photochromism

Photochromism is a reversible change of color upon exposure to light. It is well known that this phenomenon appears when Ag species interact with TiO_2. The process is similar to the one that occurs during catalysis: under UV irradiation electrons at the valence band of TiO_2 are excited into the conduction band and then migrate to Ag^+ species, reducing them to Ag^0. Then, the opposite reaction can occur: Ag NP interact with visible light through their LSPR, and electrons migrate to the conduction band of TiO_2, which induces the oxidation of Ag^0 to Ag^+ (Bois et al. 2009). The whole process is accompanied by a color change, and therefore this property can be exploited in the design of optical data storage, sensors, and display devices.

Ag@TiO_2 nanocomposite presenting photochromism was first prepared by Bois et al. in 2009 (Bois et al. 2009). They observed the disappearance of the color associated to the LSPR band upon irradiation with visible light, which was then applied to "write" and "erase" Ag NP within TiO_2 MPF by using UV and visible light (Crespo-Monteiro et al. 2010). More recently, Nadar et al. observed multicolor photochromism of Ag-containing MPF of amorphous or crystalline TiO_2 (Nadar et al. 2011, 2013). The different size distributions and localizations of the NP give rise to different photochromic behaviors when exposed to visible laser light and even the bleaching of different film colors under laser exposure (Fig. 7a). Six

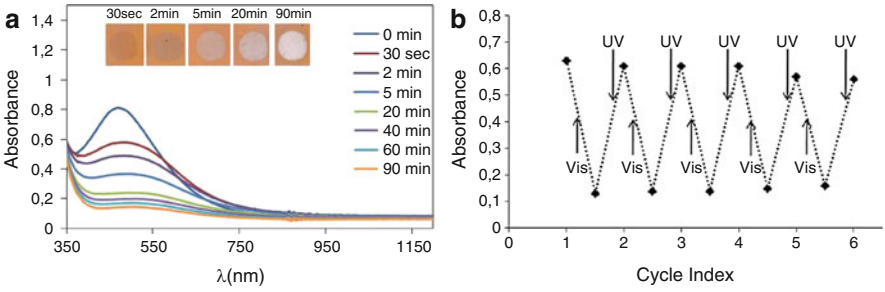

Fig. 7 (**a**) Color and UV–vis spectra after blue laser illumination for different times of Ag@TiO_2 MPF (Reproduced from (Nadar et al. 2011) with permission of The Royal Society of Chemistry). (**b**) Changes of absorbance at 488 nm for Ag@TiO_2 MPF composite, induced during six photochromic cycles by alternating ultraviolet and blue irradiation in air (Reproduced from (Nadar et al. 2013) with permission of Springer)

photochromic cycles between a bleached and a colored state were performed, showing a good repeatability of the photo-reduction/photo-oxidation processes (Fig. 7b). Moreover, it was observed that colors are stable for several months when the samples are kept off of the laser light.

Outlook and Perspectives

Metal NP and oxide MPF can be rather easily combined since the mesopores are complementary with the particles, both in size and potential applications. The obtained NP@MPF composites present the intrinsic properties of each family, but also acquire new features derived from the synergy between the components.

The diversity of synthesis approaches offers several possible configurations, with the metal NP included inside the mesopores or in the oxide framework and also completely covered by the MPF. Thus, the MPF can act as a host matrix but can also control the NP size and spatial distribution or even can be a filter or physical spacer of the surrounding environment. Besides, new properties are developed, due to the huge interfacial contact between the metal and the oxide.

The nanocomposite structure (film porosity, pore sizes, NP loading, NP size and shape, metal-oxide interfaces, etc.) determines, in most cases, the optical, catalytic, and sensing properties. In this context, a truthful material characterization using spectroscopies, electron microscopies, and X-ray based techniques is fundamental to understand the obtained properties and design novel devices based on NP@MPF.

Although the synthesis methods are well established and there is a huge palette of characterization techniques, the applications of these composites are still under development. In this chapter, we have discussed a few of them, but other fields may readily benefit from the special properties of these nanocomposites, such as environmental remediation, drug delivery, and surface protection. Future works in these directions are needed to transform some of the potential applications of these interesting materials into real devices.

Acknowledgments We thank Dr. Eduardo Martínez and M. Mercedes Zalduendo for providing the optical images presented in Fig. 2.

This work was supported by CONICET (PIP 00044CO).

References

Abalde-Cela S, Carregal-Romero S, Coelho JP, Guerrero-Martínez A. Recent progress on colloidal metal nanoparticles as signal enhancers in nanosensing. Adv Colloid Interface Sci. 2016;233:255–70.

Álvarez-Puebla RA, Liz-Marzán LM. SERS-based diagnosis and biodetection. Small. 2010;6:604–10.

Andersson M, Birkedal H, Franklin NR, Ostomel T, Boettcher S, Palmqvist AEC, Stucky GD. Ag/AgCl-loaded ordered mesoporous anatase for photocatalysis. Chem Mater. 2005;17:1409–15.

Angelomé PC, Liz-Marzán LM. Monitoring solvent evaporation from thin films by localized surface plasmon resonance shifts. J Phys Chem C. 2010;114:18379–83.
Angelomé PC, Liz-Marzán LM. Synthesis and applications of mesoporous nanocomposites containing metal nanoparticles. J Sol–gel Sci Technol. 2014;70:180–90.
Angelomé PC, Andrini L, Fuertes MC, Requejo FG, Soler-Illia GJAA. Large-pore mesoporous titania-silica thin films (Ti1-xSixO2, $0.1 \leq x \leq 0.9$) with highly interdispersed mixed oxide frameworks. C R Chim. 2010;13:256–69.
Angelomé PC, Pastoriza-Santos I, Pérez Juste J, Rodríguez-González B, Zelcer A, Soler-Illia GJAA, Liz Marzán LM. Growth and branching of gold nanoparticles through mesoporous silica thin films. Nanoscale. 2012;4:931–9.
Astruc D, Lu F, Aranzaes JR. Nanoparticles as recyclable catalysts: the frontier between homogeneous and heterogeneous catalysis. Angew Chem Int Ed. 2005;44:7852–72.
Atwater HA, Polman A. Plasmonics for improved photovoltaic devices. Nat Mater. 2010;9:205–13.
Baklanov MR, Mogilnikov KP, Polovinkin VG, Dultsev FN. Determination of pore size distribution in thin films by ellipsometric porosimetry. J Vac Sci Technol B: Microelectron Nanometer Struct. 2000;18:1385–91.
Bannat I, Wessels K, Oekermann T, Rathousky J, Bahnemann D, Wark M. Improving the photocatalytic performance of mesoporous titania films by modification with gold nanostructures. Chem Mater. 2009;21:1645–53.
Battie Y, Destouches N, Bois L, Chassagneux F, Tishchenko A, Sp P, Boukenter A. Growth mechanisms and kinetics of photoinduced silver nanoparticles in mesostructured hybrid silica films under UV and visible illumination. J Phys Chem C. 2010;114:8679–87.
Battie Y, Destouches N, Chassagneux F, Jamon D, Bois L, Moncoffre N, Toulhoat N. Optical properties of silver nanoparticles thermally grown in a mesostructured hybrid silica film. Opt Mater Express. 2011;1:1019–33.
Beck JS, Vartuli JC, Roth WJ, Leonowicz ME, Kresge CT, Schmitt KD, Chu CTW, Olson DH, Sheppard EW, McCullen SB, Higgins JB, Schlenker JL. A new family of mesoporous molecular sieves prepared with liquid crystal templates. J Am Chem Soc. 1992;114:10834–43.
Besson S, Gacoin T, Ricolleau C, Boilot J-P. Silver nanoparticle growth in 3D-hexagonal mesoporous silica films. Chem Commun. 2003;360–1.
Bohren CF, Huffman DR. Absorption and scattering of light by small particles, Wiley science paperback series. New York: Wiley -Interscience; 1983.
Bois L, Bessueille F, Chassagneux F, Battie Y, Destouches N, Hubert C, Boukenter A, Parola S. Silver nanoparticles growth in a mesoporous silica film templated with the F127 triblock copolymer. Colloids Surf A Physicochem Eng Asp. 2008;325:86–92.
Bois L, Chassagneux F, Battie Y, Bessueille F, Mollet L, Parola S, Destouches N, Toulhoat N, Moncoffre N. Chemical growth and photochromism of silver nanoparticles into a mesoporous titania template. Langmuir. 2009;26:1199–206.
Bois L, Chassagneux F, Desroches C, Battie Y, Destouches N, Gilon N, Parola S, Stéphan O. Electroless growth of silver nanoparticles into mesostructured silica block copolymer films. Langmuir. 2010;26:8729–36.
Boissiere C, Grosso D, Lepoutre S, Nicole L, Bruneau AB, Sanchez C. Porosity and mechanical properties of mesoporous thin films assessed by environmental ellipsometric porosimetry. Langmuir. 2005;21:12362–71.
Brinker CJ, Lu Y, Sellinger A, Fan H. Evaporation-induced self-assembly: nanostructures made easy. Adv Mater. 1999;11:579–85.
Bronstein LM. Nanoparticles made in mesoporous solids. In: Antonietti M, editor. Colloid chemistry I. Berlin/Heidelberg: Springer; 2003. p. 55–89. doi:10.1007/3-540-36408-0_3.
Calvo A, Fuertes MC, Yameen B, Williams FJ, Azzaroni O, Soler-Illia GJAA. Nanochemistry in confined environments: polyelectrolyte brush-assisted synthesis of gold nanoparticles inside ordered mesoporous thin films. Langmuir. 2010;26:5559–67.
Carbó-Argibay E, Rodríguez-González B. Controlled growth of colloidal gold nanoparticles: single-crystalline versus multiply-twinned particles. Isr J Chem. 2015;in press. doi: 10.1002/ijch.201500032.

Carretero-Genevrier A, Drisko GL, Grosso D, Boissiere C, Sanchez C. Mesoscopically structured nanocrystalline metal oxide thin films. Nanoscale. 2014;6:14025–43.

Chassagneux F, Bois L, Simon J-P, Desroches C, Brioude A. Elaboration and characterization of bimetallic gold-silver nanoparticles supported on mesostructured silica films. J Mater Chem. 2011a;21:11947–55.

Chassagneux F, Chiriac R, Bessueille F, Karabulut M, Bois L, Parola S. Ellipsoporosimetry and thermoporometry analyses of mesoporous titania film containing silver nanoparticles. Microporous Mesoporous Mater. 2011b;139:52–8.

Chassagneux F, Simon J-P, Bois L, Desroches C, Brioude A. Reorganization induced by silver salt reduction inside a mesostructured block copolymer silica film. J Phys Chem C. 2011c;115:25201–8.

Cortial G, Siutkowski M, Goettmann F, Moores A, Boissière C, Grosso D, Le Floch P, Sanchez C. Metallic nanoparticles hosted in mesoporous oxide thin films for catalytic applications. Small. 2006;2:1042–5.

Crespo-Monteiro N, Destouches N, Bois L, Chassagneux F, Reynaud S, Fournel T. Reversible and irreversible laser microinscription on silver-containing mesoporous titania films. Adv Mater. 2010;22:3166–70.

Crespo-Monteiro N, Destouches N, Nadar L, Reynaud S, Vocanson F, Michalon JY. Irradiance influence on the multicolor photochromism of mesoporous TiO_2 films loaded with silver nanoparticles. Appl Phys Lett. 2011;99:173106.

Cui F, Hua Z, Cui X, Guo L, Wei C, Bu W, Shi J. Au nanoparticles incorporated mesoporous silica thin films with a high Au content: preparation and third-order optical non-linearity. Dalton Trans. 2009a;2679–82.

Cui F, Hua Z, Wei C, Li Z, Gao Z, Shi J. Highly dispersed Au nanoparticles incorporated mesoporous TiO_2 thin ultrahigh Au content. J Mater Chem. 2009b;19:7632–7.

Cui F, Feng C, Xie R, Hua Z, Cui X, Zhou J, Wei C, Ohtsuka H, Sakka Y, Shi J. Significant third-order optical nonlinearity enhancement of gold nanoparticle incorporated mesoporous silica thin films by magnetic field thermal treatment. J Mater Chem. 2010;20:8399–404.

Dag O, Samarskaya O, Coombs N, Ozin GA. The synthesis of mesostructured silica films and monoliths functionalised by noble metal nanoparticles. J Mater Chem. 2003;13:328–34.

Destouches N, Battie Y, Crespo-Monteiro N, Chassagneux F, Bois L, Bakhti S, Vocanson F, Toulhoat N, Moncoffre N, Epicier T. Photo-directed organization of silver nanoparticles in mesostructured silica and titania films. J Nanopart Res C7 – 1422. 2013;15:1–10.

Destouches N, Crespo-Monteiro N, Vitrant G, Lefkir Y, Reynaud S, Epicier T, Liu Y, Vocanson F, Pigeon F. Self-organized growth of metallic nanoparticles in a thin film under homogeneous and continuous-wave light excitation. J Mater Chem C. 2014;2:6256–63.

Ding L, Li W, Sun Q, He Y, Su B. Gold nanoparticles confined in vertically aligned silica nanochannels and their electrocatalytic activity toward ascorbic acid. Chem A Eur J. 2014;20:12777–80.

Doane TL, Burda C. The unique role of nanoparticles in nanomedicine: imaging, drug delivery and therapy. Chem Soc Rev. 2012;41:2885–911.

Fang J-Y, Qin S-Q, Zhang X-A, Nie Y-M, Wang F. Linear and nonlinear optical properties of gold nanocrystal-incorporated mesoporous silica thin films. RSC Adv. 2012;2:11777–85.

Fuertes MC, Marchena M, Marchi MC, Wolosiuk A, Soler-Illia GJAA. Controlled deposition of silver nanoparticles in mesoporous single- or multilayer thin films: from tuned pore filling to selective spatial location of nanometric objects. Small. 2009;5:272–80.

Fukuoka A, Araki H, Sakamoto Y, Sugimoto N, Tsukada H, Kumai Y, Akimoto Y, Ichikawa M. Template synthesis of nanoparticle arrays of gold and platinum in mesoporous silica films. Nano Lett. 2002;2:793–5.

Fukuoka A, Araki H, Kimura J-I, Sakamoto Y, Higuchi T, Sugimoto N, Inagaki S, Ichikawa M. Template synthesis of nanoparticle arrays of gold, platinum and palladium in mesoporous silica films and powders. J Mater Chem. 2004;14:752–6.

Gibaud A, Dourdain S, Vignaud G. Analysis of mesoporous thin films by X-ray reflectivity, optical reflectivity and grazing incidence small angle X-ray scattering. Appl Surf Sci. 2006;253:3–11.

Goettmann F, Moores A, Boissière C, Le Floch P, Sanchez C. A selective chemical sensor based on plasmonic response of phosphinine-stabilized gold nanoparticles hosted on periodically organized mesoporous silica thin layers. Small. 2005;1:636–9.

Grzelczak M, Pérez Juste J, Mulvaney P, Liz Marzán LM. Shape control in gold nanoparticle synthesis. Chem Soc Rev. 2008;37:1783–91.

Gu D, Schuth F. Synthesis of non-siliceous mesoporous oxides. Chem Soc Rev. 2014;43:313–44.

Gu J, Shi J, Xiong L, Chen H, Ruan M. A new strategy to incorporate highly dispersed nanoparticles into the pore channels of mesoporous silica thin films. Microporous Mesoporous Mater. 2004;74:199–204.

Gu JL, Shi JL, You GJ, Xiong LM, Qian SX, Hua ZL, Chen HR. Incorporation of highly dispersed gold nanoparticles into the pore channel of mesoporous silica thin films and their ultrafast nonlinear optical response. Adv Mater. 2005;17:557–60.

Hamanaka Y, Fukuta K, Nakamura A, Liz-Marzán LM, Mulvaney P. Enhancement of third-order nonlinear optical susceptibilities in silica-capped Au nanoparticle films with very high concentrations. Appl Phys Lett. 2004;84:4938–40.

Horiuchi Y, Shimada M, Kamegawa T, Mori K, Yamashita H. Size-controlled synthesis of silver nanoparticles on Ti-containing mesoporous silica thin film and photoluminescence enhancement of rhodamine 6G dyes by surface plasmon resonance. J Mater Chem. 2009;19:6745–9.

Howes PD, Rana S, Stevens MM. Plasmonic nanomaterials for biodiagnostics. Chem Soc Rev. 2014;43:3835–53.

Hu J, Wang L, Cai W, Li Y, Zeng H, Zhao L, Liu P. Smart and reversible surface Plasmon resonance responses to various atmospheres for silver nanoparticles loaded in mesoporous SiO_2. J Phys Chem C. 2009;113:19039–45.

Innocenzi P, Malfatti L. Mesoporous thin films: properties and applications. Chem Soc Rev. 2013;42:4198–216.

Jimenez de Aberasturi D, Serrano-Montes AB, Liz-Marzán LM. Modern applications of plasmonic nanoparticles: from energy to health. Adv Opt Mater. 2015;3:602–17.

Kanno Y, Suzuki T, Yamauchi Y, Kuroda K. Preparation of Au nanowire films by electrodeposition using mesoporous silica films as a template: vital effect of vertically oriented mesopores on a substrate. J Phys Chem C. 2012;116:24672–80.

Kobayashi Y, Correa-Duarte MA, Liz-Marzán LM. Sol–gel processing of silica-coated gold nanoparticles. Langmuir. 2001;17:6375–9.

Kreibig U, Vollmer M. Optical properties of metal clusters, Springer series in materials science. Berlin: Springer; 1995.

Kresge CT, Roth WJ. The discovery of mesoporous molecular sieves from the twenty year perspective. Chem Soc Rev. 2013;42:3663–70.

Kresge CT, Leonowicz ME, Roth WJ, Vartuli JC, Beck JS. Ordered mesoporous molecular sieves synthesized by a liquid-crystal template mechanism. Nature. 1992;359:710–2.

Krylova GV, Gnatyuk YI, Smirnova NP, Eremenko AM, Gun'ko VM. Ag nanoparticles deposited onto silica, titania, and zirconia mesoporous films synthesized by sol–gel template method. J Sol–gel Sci Technol. 2009;50:216–28.

Kumai Y, Tsukada H, Akimoto Y, Sugimoto N, Seno Y, Fukuoka A, Ichikawa M, Inagaki S. Highly ordered platinum nanodot arrays with cubic symmetry in mesoporous thin films. Adv Mater. 2006;18:760–2.

Lebeau B, Galarneau A, Linden M. Introduction for 20 years of research on ordered mesoporous materials. Chem Soc Rev. 2013;42:3661–2.

Leroy CM, Cardinal T, Jubera V, Aymonier C, Treguer-Delapierre M, Boissière C, Grosso D, Sanchez C, Viana B, Pellé F. Luminescence properties of ZrO2 mesoporous thin films doped with Eu3+ and Agn. Microporous Mesoporous Mater. 2013;170:123–30.

Li N, Zhao P, Astruc D. Anisotropic gold nanoparticles: synthesis, properties, applications, and toxicity. Angew Chem Int Ed. 2014a;53:1756–89.

Li W, Wu Z, Wang J, Elzatahry AA, Zhao D. A perspective on mesoporous TiO_2 materials. Chem Mater. 2014b;26:287–98.

Liao HB, Xiao RF, Fu JS, Yu P, Wong GKL, Sheng P. Large third-order optical nonlinearity in Au: SiO_2 composite films near the percolation threshold. Appl Phys Lett. 1997;70:1–3.

Liu Z, Destouches N, Vitrant G, Lefkir Y, Epicier T, Vocanson F, Bakhti S, Fang Y, Bandyopadhyay B, Ahmed M. Understanding the growth mechanisms of Ag nanoparticles controlled by Plasmon-induced charge transfers in Ag-TiO_2 films. J Phys Chem C. 2015;119:9496–505.

Liz-Marzán LM. Tailoring surface plasmons through the morphology and assembly of metal nanoparticles. Langmuir. 2006;22:32–41.

López-Puente V, Abalde-Cela S, Angelomé PC, Alvarez-Puebla RA, Liz-Marzán LM. Plasmonic mesoporous composites as molecular sieves for SERS detection. J Phys Chem Lett. 2013;4:2715–20.

López-Puente V, Angelomé PC, Soler-Illia GJAA, Liz-Marzán LM. Selective SERS sensing modulated by functionalized mesoporous films. ACS Appl Mater Interfaces. 2015;7: 25633–40.

Losurdo M, Bergmair M, Bruno G, Cattelan D, Cobet C, Martino A, Fleischer K, Dohcevic-Mitrovic Z, Esser N, Galliet M, Gajic R, Hemzal D, Hingerl K, Humlicek J, Ossikovski R, Popovic ZV, Saxl O. Spectroscopic ellipsometry and polarimetry for materials and systems analysis at the nanometer scale: state-of-the-art, potential, and perspectives. J Nanopart Res. 2009;11:1521–54.

Lu Q, Cui F, Dong C, Hua Z, Shi J. Gold nanoparticles incorporated mesoporous silica thin films of varied gold contents and their well-tuned third-order optical nonlinearities. Opt Mater. 2011;33:1266–71.

Malfatti L, Marongiu D, Costacurta S, Falcaro P, Amenitsch H, Marmiroli B, Grenci G, Casula MF, Innocenzi P. Writing self-assembled mesostructured films with in situ formation of gold nanoparticles. Chem Mater. 2010;22:2132–7.

Malfatti L, Falcaro P, Marmiroli B, Amenitsch H, Piccinini M, Falqui A, Innocenzi P. Nanocomposite mesoporous ordered films for lab-on-chip intrinsic surface enhanced Raman scattering detection. Nanoscale. 2011;3:3760–6.

Martínez ED, Bellino MG, Soler-Illia GJAA. Patterned production of silver-mesoporous titania nanocomposite thin films using lithography-assisted metal reduction. ACS Appl Mater Interfaces. 2009;1:746–9.

Martinez ED, Granja L, Bellino MG, Soler-Illia GJAA. Electrical conductivity in patterned silver-mesoporous titania nanocomposite thin films: towards robust 3D nano-electrodes. Phys Chem Chem Phys. 2010;12:14445–8.

Martínez ED, Boissière C, Grosso D, Sanchez C, Troiani H, Soler-Illia GJAA. Confinement-induced growth of Au nanoparticles entrapped in mesoporous TiO_2 thin films evidenced by in situ thermo-ellipsometry. J Phys Chem C. 2014;118:13137–51.

May RA, Patel MN, Johnston KP, Stevenson KJ. Flow-based multiadsorbate ellipsometric porosimetry for the characterization of mesoporous Pt-TiO_2 and Au-TiO_2 nanocomposites. Langmuir. 2009;25:4498–509.

Mitra A, Jana D, De G. A facile synthesis of cubic Im(−3)m alumina films on glass with potential catalytic activity. Chem Commun. 2012;48:3333–5.

Moores A, Goettmann F. The plasmon band in noble metal nanoparticles: an introduction to theory and applications. New J Chem. 2006;30:1121–32.

Muraza O, Rebrov EV, Berenguer-Murcia A, de Croon MHJM, Schouten JC. Selectivity control in hydrogenation reactions by nanoconfinement of polymetallic nanoparticles in mesoporous thin films. Appl Catal A Gen. 2009;368:87–96.

Myroshnychenko V, Rodríguez-Fernández J, Pastoriza-Santos I, Funston AM, Novo C, Mulvaney P, Liz-Marzán LM, García de Abajo FJ. Modelling the optical response of gold nanoparticles. Chem Soc Rev. 2008;37:1792–805.

Nadar L, Sayah R, Vocanson F, Crespo-Monteiro N, Boukenter A, Sao Joao S, Destouches N. Influence of reduction processes on the colour and photochromism of amorphous mesoporous TiO_2 thin films loaded with a silver salt. Photochem Photobiol Sci. 2011;10:1810–6.

Nadar L, Destouches N, Crespo-Monteiro N, Sayah R, Vocanson F, Reynaud S, Lefkir Y, Capoen B. Multicolor photochromism of silver-containing mesoporous films of amorphous or anatase TiO_2. J Nanopart Res. 2013;15:1–10.

Oates TWH, Wormeester H, Arwin H. Characterization of plasmonic effects in thin films and metamaterials using spectroscopic ellipsometry. Prog Surf Sci. 2011;86:328–76.

Pastoriza-Santos I, Liz-Marzán LM. Colloidal silver nanoplates. State of the art and future challenges. J Mater Chem. 2008;18:1724–37.

Patel MN, Williams RD, May RA, Uchida H, Stevenson KJ, Johnston KP. Electrophoretic deposition of Au nanocrystals inside perpendicular mesochannels of TiO_2. Chem Mater. 2008;20:6029–40.

Pedrueza E, Valdés JL, Chirvony V, Abargues R, Hernández-Saz J, Herrera M, Molina SI, Martínez-Pastor JP. Novel method of preparation of gold-nanoparticle-doped TiO_2 and SiO_2 plasmonic thin films: optical characterization and comparison with Maxwell–Garnett modeling. Adv Funct Mater. 2011;21:3502–7.

Pérez MD, Otal E, Bilmes SA, Soler-Illia GJAA, Crepaldi EL, Grosso D, Sanchez C. Growth of gold nanoparticle arrays in TiO_2 mesoporous matrixes. Langmuir. 2004;20:6879–86.

Pérez-Juste J, Correa-Duarte MA, Liz-Marzán LM. Silica gels with tailored, gold nanorod-driven optical functionalities. Appl Surf Sci. 2004;226:137–43.

Petkov N, Platschek B, Morris MA, Holmes JD, Bein T. Oriented growth of metal and semiconductor nanostructures within aligned mesoporous channels. Chem Mater. 2007;19:1376–81.

Plyuto Y, Berquier J-M, Jacquiod C, Ricolleau C. Ag nanoparticles synthesised in template-structured mesoporous silica films on a glass substrate. Chem Commun. 1999;1653–4.

Qi H, Shopsowitz KE, Hamad WY, MacLachlan MJ. Chiral nematic assemblies of silver nanoparticles in mesoporous silica thin films. J Am Chem Soc. 2011;133:3728–31.

Rafti M, Brunsen A, Fuertes MC, Azzaroni O, Soler-Illia GJAA. Heterogeneous catalytic activity of platinum nanoparticles hosted in mesoporous silica thin films modified with polyelectrolyte brushes. ACS Appl Mater Interfaces. 2013;5:8833–40.

Roldán MV, de Oña P, Castro Y, Durán A, Faccendini P, Lagier C, Grau R, Pellegri NS. Photocatalytic and biocidal activities of novel coating systems of mesoporous and dense TiO_2-anatase containing silver nanoparticles. Mater Sci Eng C. 2014;43:630–40.

Roldán MV, Castro Y, Pellegri N, Durán A. Enhanced photocatalytic activity of mesoporous SiO_2/TiO_2 sol–gel coatings doped with Ag nanoparticles. J Sol–gel Sci Technol. 2015;76:180–94.

Sánchez C, Boissière C, Grosso D, Laberty C, Nicole L. Design, synthesis, and properties of inorganic and hybrid thin films having periodically organized nanoporosity. Chem Mater. 2008;20:682–737.

Sánchez VM, Martínez ED, Martínez Ricci ML, Troiani H, Soler-Illia GJAA. Optical properties of Au nanoparticles included in mesoporous TiO_2 thin films: a dual experimental and modeling study. J Phys Chem C. 2013;117:7246–59.

Sayah R, Nadar L, Vocanson F, Battie Y, Reynaud S, Vera R, Boukenter A, Destouches N. Growth by heat treatment of silver nanorods inside mesostructured silica thin films: Synthesis, colours of thin films, study of some experimental parameters and characterization. Microporous Mesoporous Mater. 2011;139:45–51.

Schätz A, Reiser O, Stark WJ. Nanoparticles as semi-heterogeneous catalyst supports. Chem A Eur J. 2010;16:8950–67.

Schlücker S. Surface-enhanced Raman spectroscopy: concepts and chemical applications. Angew Chem Int Ed. 2014;53:4756–95.

Selvan ST, Hayakawa T, Nogami M, Kobayashi Y, Liz-Marzán LM, Hamanaka Y, Nakamura A. Sol–gel derived gold nanoclusters in silica glass possessing large optical nonlinearities. J Phys Chem B. 2002;106:10157–62.

Sepúlveda B, Angelomé PC, Lechuga LM, Liz-Marzán LM. LSPR-based nanobiosensors. Nano Today. 2009;4:244–51.

Soler-Illia GJAA, Innocenzi P. Mesoporous hybrid thin films: the physics and chemistry beneath. Chem A Eur J. 2006;12:4478–94.

Soler-Illia GJAA, Angelomé PC, Fuertes MC, Grosso D, Boissiere C. Critical aspects in the production of periodically ordered mesoporous titania thin films. Nanoscale. 2012;4:2549–66.
Sperling RA, Rivera Gil P, Zhang F, Zanella M, Parak WJ. Biological applications of gold nanoparticles. Chem Soc Rev. 2008;37:1896–908.
Sun J, Bao X. Textural manipulation of mesoporous materials for hosting of metallic nanocatalysts. Chem A Eur J. 2008;14:7478–88.
Thomas JM, Terasaki O, Gai PL, Zhou W, Gonzalez-Calbet J. Structural elucidation of microporous and mesoporous catalysts and molecular sieves by high-resolution electron microscopy. Acc Chem Res. 2001;34:583–94.
Tompkins HG, McGahan WA. Spectroscopic ellipsometry and reflectometry. A user's guide. New York: Wiley Interscience; 1999.
van der Lee A. Grazing incidence specular reflectivity: theory, experiment, and applications. Solid State Sci. 2000;2:257–78.
Violi IL, Zelcer A, Bruno MM, Luca V, Soler-Illia GJAA. Gold nanoparticles supported in zirconia-ceria mesoporous thin films: a highly active reusable heterogeneous nanocatalyst. ACS Appl Mater Interfaces. 2015;7:1114–21.
White RJ, Luque R, Budarin VL, Clark JH, Macquarrie DJ. Supported metal nanoparticles on porous materials. Methods and applications. Chem Soc Rev. 2009;38:481–94.
Wolosiuk A, Tognalli NG, Martínez ED, Granada M, Fuertes MC, Troiani H, Bilmes SA, Fainstein A, Soler-Illia GJAA. Silver nanoparticle-mesoporous oxide nanocomposite thin films: a platform for spatially homogeneous SERS-active substrates with enhanced stability. ACS Appl Mater Interfaces. 2014;6:5263–72.
Wu C-W, Yamauchi Y, Ohsuna T, Kuroda K. Structural study of highly ordered mesoporous silica thin films and replicated Pt nanowires by high-resolution scanning electron microscopy (HRSEM). J Mater Chem. 2006;16:3091–8.
Xia Y, Xiong Y, Lim B, Skrabalak SE. Shape-controlled synthesis of metal nanocrystals: simple chemistry meets complex physics? Angew Chem Int Ed. 2009;48:60–103.
Xia X, Zeng J, Zhang Q, Moran CH, Xia Y. Recent developments in shape-controlled synthesis of silver nanocrystals. J Phys Chem C. 2012;116:21647–56.
Yacou C, Fontaine M-L, Ayral A, Lacroix-Desmazes P, Albouy P-A, Julbe A. One pot synthesis of hierarchical porous silica membrane material with dispersed Pt nanoparticles using a microwave-assisted sol–gel route. J Mater Chem. 2008;18:4274–9.
Yang Z, Ni W, Kou X, Zhang S, Sun Z, Sun L-D, Wang J, Yan C-H. Incorporation of gold nanorods and their enhancement of fluorescence in mesostructured silica thin films. J Phys Chem C. 2008;112:18895–903.
Zhang Y, Yuwono AH, Li J, Wang J. Highly dispersed gold nanoparticles assembled in mesoporous titania films of cubic configuration. Microporous Mesoporous Mater. 2008;110:242–9.
Zhao J, Sallard S, Smarsly BM, Gross S, Bertino M, Boissiere C, Chen H, Shi J. Photocatalytic performances of mesoporous TiO_2 films doped with gold clusters. J Mater Chem. 2010;20:2831–9.
Zhao P, Li N, Astruc D. State of the art in gold nanoparticle synthesis. Coord Chem Rev. 2013;257:638–65.